A.V. BABICH
Zaporizhzhya National Technical University
(64, Zhukovskii Str., Zaporizhzhya 60063, Ukraine; e-mail: andrei_babich@mail.ru)

ON THE WORK FUNCTION AND SCHOTTKY BARRIER HEIGHTS OF METAL NANOFILMS IN A DIELECTRIC ENVIRONMENT

UDC 537.533.2: 539.37

We suggest a method for self-consistent calculations of the characteristics of metal films in a dielectric environment. Within a modified Kohn–Sham method and the stabilized jellium model, the most interesting case of asymmetric metal-dielectric sandwiches is considered, for which the dielectric media are different on the two sides of the film. We calculate the spectrum, electron work function, and surface energy of polycrystalline and crystalline films of Na, Al, and Pb placed into passive isolators. It is found that a dielectric environment generally leads to a decrease of both the electron work function and the surface energy. It is revealed that the change of the work function is determined only by the average of dielectric constants on both sides of the film. We introduced the position of a conduction band in the dielectric as a parameter in the self-consistency procedure. The calculations with the use of the image potential for an aluminum film with ideal interfaces vacuum/Al(111)/SiO_2 and vacuum/Al(111)/Al_2O_3 and the sandwich SiO_2/Al(111)/Al_2O_3 are performed. As a result, the effective potential profiles and the Schottky barrier heights are calculated.

Keywords: metal nanofilm, dielectric, work function, surface energy, Schottky barrier height.

1. Introduction

Thin metal films and flat islands on semiconductor or dielectric substrates can be considered as two-dimensional electron systems with properties, which are of interest both from the fundamental point of view and from the perspective of their application to nanoscale electronic devices.

There are a limited number of experimental works focused on quantum size effects in such systems (for reviews, see [1–9]) due to difficulties in the fabrication of samples, as well as because of the lack of suitable experimental methods. One of the most important characteristics of metal nanostructures is the electron work function.

As a rule, the calculations of electron work functions for films are performed for the idealized case of films in vacuum. Similarly to clusters, the work function defines an ionization potential. There are different methods, which enable one to calculate the electron structure of slabs (in vacuum) consisting of a few monoatomic layers (ML). Let us combine them into three groups according to the complexity of computations: I – Sommerfeld electrons in the box model (analytical calculations, slabs and wires) [10–15]; II – self-consistent calculations within various versions of the jellium model (slabs and wires) [16–20]; III – *ab initio* calculations (slabs) [21–24]. The obtained results are illustrated in Fig. 1 for all these three groups. An important ingredient of approaches within group III is the monolayer number in the film (see dots in Fig. 1). For groups I and II, L changes continuously.

In group I, the Fermi energy (kinetic energy) $\varepsilon_{\rm F}(L)$ is reckoned from the *flat* bottom of the conduction band, while the work function $W(L)$ is reckoned from the vacuum level. Therefore, their size dependences are "asymmetric". In addition to quantum oscillations, these quantities contain monotonic size contributions, which, at small film thicknesses, *together* show up through inequalities $0 < W(L) < W_0$ and $\varepsilon_{\rm F}(L) > \bar{\varepsilon}_{\rm F} > 0$, where W_0 and $\bar{\varepsilon}_{\rm F}$ correspond to a three-dimensional (3D) metal (allowing for the energy counting for $\bar{\varepsilon}_{\rm F}$).

In [25,26], the asymptotic behavior of the electron chemical potential for spherical clusters of radius R was determined. It yields

$$W(R) = W_0 - \frac{c_1}{R} < W_0, \qquad (1)$$

where $c_1 \simeq 2.5\,\text{eV} \times a_0$ for simple metals, and $a_0 = \hbar^2/(me^2)$. It is expectable that such a monotonic contribution must appear for films as well. However, in contrast to the case of group I, the self-consistent calculations of groups II and III (see Fig. 1) at small film thicknesses point out to the suppression of the monotonic dependence (with asymptotic (1)) by corrections of higher orders of smallness. For instance, the compensation of terms $-c_1/L + c_2/L^2$ occurs at $L^* = c_2/c_1$, and L^* is large, provided $c_2 \gg c_1 > 0$.

The experimental results also do not allow one to draw unambiguous conclusions on the character of the monotonic component of $W(L)$: in experiments [3], it is absent (Yb films on Si substrate), while, according to [2, 5], it coincides with the one of group I. Note that the comparison of a measured work function for the sandwich consisting of an Ag film on Fe(100) in [2, 5] with calculated results for slabs *in vacuum* is rather relative.

Let the film placed on a substrate be considered. In order to determine the characteristics of contacts in the easiest case, it is necessary to know the dielectric constant ϵ as well as the position of the conduction band $-\chi$ (χ is the electron affinity) in a dielectric material. The approximation $\chi = 0$ was widely used for the work function, polarizability, and surface plasmon resonance of jellium spheres and wires embedded in different dielectric matrices (see [19, 27–29] and references therein).

The aim of this work is to compute the energy characteristics of metal films in dielectrics. A method for self-consistent calculations of the equilibrium profiles of the electron concentration, effective potential, energy spectrum, and integral characteristics of metal films in dielectrics and dielectric substrates is suggested. The developed method is based on the stabilized jellium model [30] and the local density approximation for an exchange-correlation potential [31], which were used by us [32] to analyze the characteristics of a semi-infinite metal with dielectric coating. For our problem, in the spirit of Serena *et al.* [33], we introduce a nonlocal potential matched at the image-plane positions to the local exchange-correlation potential. We also introduce the position of a conduction band in the dielectric as a parameter in the self-consistency procedure and perform calculations of the effective potential profiles and the Schottky barrier heights for the

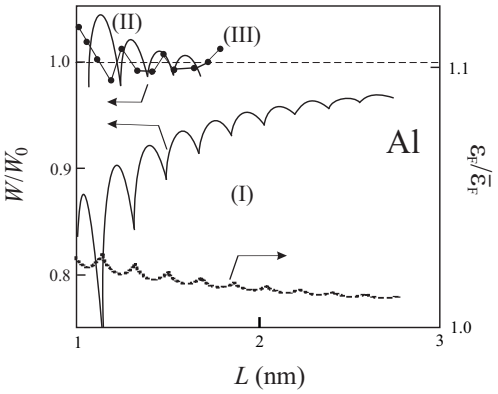

Fig. 1. Illustration of the computation results for groups I, II, and III (data for group I are deduced from [12])

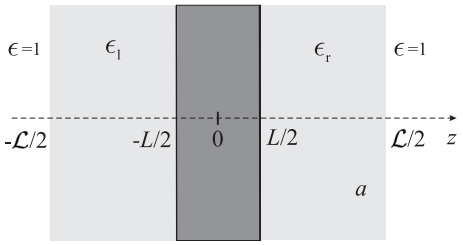

Fig. 2. Scheme of a film in the dielectric environment

vacuum/Al(111)/SiO_2 and vacuum/Al(111)/Al_2O_3 and the sandwich SiO_2/Al(111)/Al_2O_3.

This paper is organized as follows. In Section II, we formulate our model. In Section III, we present our main results and provide a discussion of them. The conclusions are drawn in Section IV.

2. Model

Let us consider a metallic film of thickness L at zero temperature. We direct the z-axis perpendicularly to the film surface (Fig. 2, $\mathcal{L} \gg L$).

The main identities for a film can be obtained within the model of a rectangular well for conduction electrons. To perform a preliminary analysis, we suppose that the bottom of the potential well is flat, and we reckon energies starting from its value. The final expression for the kinetic energies of conduction electrons depends only on energy differences; therefore, the counting of energies in such a way is allowable.

We study a film of thickness L comparable in magnitude to the Fermi wavelength $\bar{\lambda}_F = 2\pi/\bar{k}_F$ of an electron in a 3D metal. The longitudinal sizes of the sample are assumed to be considerably larger than

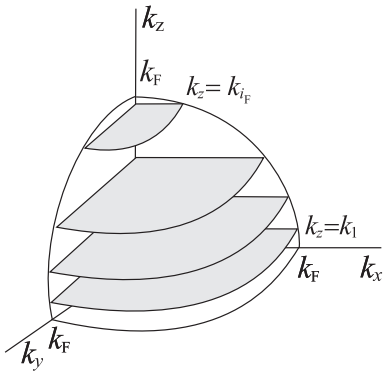

Fig. 3. Scheme for the occupation of electronic states in the k space

the film thickness ($L \ll L_x$, L_y), which leads to the pronounced quantization of the transverse component of the electron momentum. The three-dimensional Schrödinger equation for a quantum box can be separated into one-dimensional equations.

The eigenenergies are given by

$$\varepsilon_{ik_\parallel} = \varepsilon_i + \frac{k_\parallel^2}{2}, \quad k_\parallel^2 = k_x^2 + k_y^2, \tag{2}$$

where ε_i is the eigenvalue of the i-th perpendicular state $\psi_i(z)$ (hereafter, the Hartree atomic units are used: $\hbar = m = e = 1$). The eigenvalue ε_i is the bottom of the i-th subband. For finite and periodic systems in the z-direction, the Dirichlet and periodic boundary conditions are used, respectively. Therefore, possible allowed electron states k_x, k_y, k_z form a system of parallel planes in the k-space, $k_z \equiv k_i$.

The occupation of electron states starts from the point $\{0, 0, k_1\}$ and follows an increase of the radius-vector. As a result, it turns out that all occupied states are contained within the area of the k-space confined between the plane $k_z = k_1$ and a semi-sphere of the radius $k_F = \sqrt{2\varepsilon_F}$ (see Fig. 3).

The number of states dZ in each of the circles formed by the intersection of the Fermi semisphere with the planes $k_z = k_i$ of the area $S = L_x L_y$, within the interval of wave vectors $(k_\parallel, k_\parallel + dk_\parallel)$ and taking both possible spin projections into account, is $dZ(k_\parallel) = 2Sd(\pi k_\parallel^2)/(2\pi)^2$. The maximum value of $k_\parallel$ in each circle numbered by i is equal to the circle radius $k_{F(i)} = (k_F^2 - k_i^2)^{1/2}$. In order to find the number of occupied states, which coincides with the number of valence electrons N in the film, one should integrate dZ over $k_\parallel$ in each circle, and then sum up the contributions of all circles:

$$N = \frac{S}{\pi} \sum_{i=1}^{i_F} \int_0^{k_{F(i)}} dk_\parallel \, k_\parallel = \frac{S}{2\pi} \left(i_F k_F^2 - \sum_{i=1}^{i_F} k_i^2 \right). \tag{3}$$

With regard for the electron kinetic energy $\frac{1}{2}(k_\parallel^2 + k_i^2)$, the total kinetic energy of the electron subsystem equals

$$T_s = \frac{S}{2\pi} \sum_{i=1}^{i_F} \int_0^{k_{F(i)}} dk_\parallel k_\parallel \left(k_\parallel^2 + k_i^2 \right) =$$

$$= \frac{S}{4\pi} \sum_{i=1}^{i_F} k_{F(i)}^2 \left(\frac{k_{F(i)}^2}{2} + k_i^2 \right), \tag{4}$$

where i_F is the number of the last occupied or partially occupied subband.

In the frame of the density-functional theory and the stabilized jellium model (SJ), the total energy of a metal sample is represented by the functional of the inhomogeneous electron concentration $n(\mathbf{r})$:

$$E_{SJ}[n(\mathbf{r})] = T_s + E_{xc} + E_H + E_{ps} + E_M, \tag{5}$$

where T_s is the (non-interacting) electron kinetic energy, E_{xc} is the exchange-correlation energy, E_H is the Hartree (electrostatic) energy, E_{ps} is the pseudopotential (Ashcroft) correction, and E_M is the Madelung energy. The sum of first three terms in expression (5) corresponds to the "ordinary" jellium energy E_J. The average energy per valence electron in the bulk of a metal is $\bar{\varepsilon}_{SJ,J} = E_{SJ,J}[\bar{n}]/N$, where N is the total number of free electrons with concentration $\bar{n}$ defined by the valence and the atomic density.

The positive (ionic) charge distribution can be modeled by the step function

$$\rho(z) = \bar{n}\theta(L/2 - |z|). \tag{6}$$

Solving the Kohn–Sham equations

$$-\frac{1}{2}\nabla^2 \psi_i(z) + v_{eff}[z, n(z)]\psi_i(z) = \varepsilon_i \psi_i(z), \tag{7}$$

$$v_{eff}[z, n(z)] = \phi(z) + v_{xc}(z) + \langle \delta v \rangle_{face} \theta(L/2 - |z|) \tag{8}$$

together with the Poisson equation

$$\nabla^2 \phi(z) = -\frac{4\pi}{f(z)}[n(z) - \rho(z)], \tag{9}$$

with the step function

$$f(z)=\begin{cases}1; & z<-\mathcal{L}/2,\ |z|<L/2,\ z>\mathcal{L}/2,\\ \epsilon_{\rm l}; & -\mathcal{L}/2<z<-L/2,\\ \epsilon_{\rm r}; & L/2<z<\mathcal{L}/2,\end{cases} \tag{10}$$

we obtain the single-electron wave function and the eigenvalue ε_i self-consistently.

It is generally believed that the more "physical" the potential, the better the result of computations for the location of the Fermi energy (as the eigenvalue of the highest occupied state). One of the limitations of the method of effective potentials in LDA is its failure in reproducing a correct behavior of image potentials outside metal surfaces (see [34,35] and references therein). Therefore, we introduce the nonlocal potential $v_{\rm xc}^{\rm NL}(z)$ matched at the image-plane positions to the local exchange-correlation potential $v_{\rm xc}^{\rm LD}(z)=$ $=d[n(z)\varepsilon_{\rm xc}(z)]/dn(z)$ in the spirit of work [33]:

$$v_{\rm xc}(z)=\begin{cases}v_{\rm xc}^{\rm NL,l}(z), & z\le Z^{\rm l},\\ v_{\rm xc}^{\rm LD}(z), & Z^{\rm l}\le z\le Z^{\rm r},\\ v_{\rm xc}^{\rm NL,r}(z), & z\ge Z^{\rm r},\end{cases} \tag{11}$$

where $Z^{\rm l}=-L/2-z_0^{\rm l}$, $Z^{\rm r}=L/2+z_0^{\rm r}$, and the image-plane positions ($z_0^{\rm l,r}>0$) are reckoned from the left and right sides of film surfaces,

$$v_{\rm xc}^{\rm NL,l}=-\chi^{\rm l}+\frac{1-\left[1-\frac{z-Z^{\rm l}}{4\lambda_{\rm l}}\right]e^{(z-Z^{\rm l})/\lambda_{\rm l}}}{4\epsilon_{\rm l}(z-Z^{\rm l})}, \tag{12}$$

$$v_{\rm xc}^{\rm NL,r}=-\chi^{\rm r}-\frac{1-\left[1+\frac{z-Z^{\rm r}}{4\lambda_{\rm r}}\right]e^{-(z-Z^{\rm r})/\lambda_{\rm r}}}{4\epsilon_{\rm r}(z-Z^{\rm r})}. \tag{13}$$

For instance, far from the surface, (13) has a correct asymptotic behavior $\{-\chi^{\rm r}-[4\epsilon_{\rm r}(z-Z^{\rm r})]^{-1}\}$, which is an image potential. From the condition of the matching of potential (11), as well as its first derivatives in the image planes from left and right sides, we obtain simple relations:

$$\lambda_{\rm l,r}=-\frac{3}{16\epsilon_{\rm l,r}[v_{\rm xc}^{\rm LD}(Z^{\rm l,r})+\chi^{\rm l,r}]}, \tag{14}$$

$$\frac{\left|dv_{\rm xc}^{\rm LD}(z)/dz\right|_{z=Z^{\rm l,r}}}{[v_{\rm xc}^{\rm LD}(Z^{\rm l,r})+\chi^{\rm l,r}]^2}=\frac{16}{9}\epsilon_{\rm l,r}. \tag{15}$$

The relation in (15) is treated as an equation for $z_0^{\rm l,r}$. The values of $z_0^{\rm l,r}$ at the left and right sides out of the film are calculated self-consistently by solving the Kohn–Sham equations at each iteration. In this way, the effective potential is matched self-consistently to its image-potential-like form at large distances. The result of work [33] for the semiinfinite metal is reproduced for $\epsilon=1$ and $\chi=0$.

The term $\langle\delta v\rangle_{\rm face}$ in (8), which makes it possible to distinguish different crystal faces, represents the difference between the potential of the ionic lattice and the electrostatic potential of the positively charged background averaged over the Wigner–Seitz cell:

$$\langle\delta v\rangle_{\rm face}=\langle\delta v\rangle_{\rm WS}-\left(\frac{\bar{\varepsilon}_{\rm M}}{3}+\frac{\pi\bar{n}}{6}d^2\right),$$

$$\langle\delta v\rangle_{\rm WS}=-\bar{n}\frac{d\varepsilon_{\rm J}}{d\bar{n}},$$

where d is the distance between the atomic planes parallel to the surface. The term $\langle\delta v\rangle_{\rm WS}$ describes a polycrystalline sample [30]. In Eq. (10), $\epsilon_{\rm l}$ and $\epsilon_{\rm r}$ are dielectric constants of isolators from the left and right side of the film, respectively.

The electron density profile $n(z)$ is expressed in terms of the wave functions $\psi_i(z)$ as

$$n(z)=\frac{1}{2\pi}\sum_{i=1}^{i_{\rm F}}k_{{\rm F}(i)}^2\frac{|\psi_i(z)|^2}{\int_{-\infty}^{+\infty}dz\,|\psi_i(z)|^2}. \tag{16}$$

The values of $i_{\rm F}$ and $\varepsilon_{\rm F}$ are determined by solving the equation

$$\pi L\bar{n}+\sum_{i=1}^{i_{\rm F}}\varepsilon_i-i_{\rm F}\varepsilon_{\rm F}=0;\ \varepsilon_i\le\varepsilon_{\rm F};\ i=1,2,...,i_{\rm F}, \tag{17}$$

which follows from the normalization condition (3) and definition of the Fermi energy. In this equation, the integration over $k_{\|}$ is already performed, and, therefore, the summation is made only over the subband number.

In nanofilms, the spatial oscillation of the electronic density is significant throughout the sample. Therefore, the energies are reckoned from the vacuum level, which is the energy of the electron in rest in the area $|z|\gg\mathcal{L}/2$. For bound states, the energies are negative, including $\varepsilon_{\rm F}$.

We use the iterative procedure (see Appendix A) allowing us to solve self-consistently the system of equations (7), (9), (16) and to find the optimal profiles $n(z)$, $\phi(z)$, as well as the spectrum of one-particle energies. As a result, the metal/vacuum and

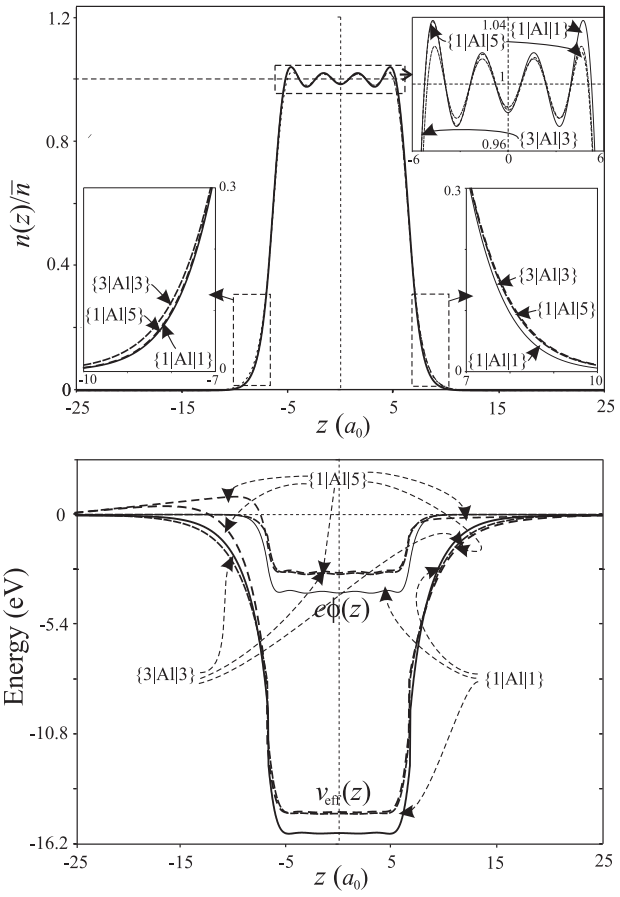

Fig. 4. Results of self-consistent calculations of the profiles of the electron density $n(z)/\bar{n}$, the one-electron effective potential $v_{\rm eff}(z)$, and the electrostatic potential $\phi(z)$ for sandwiches: $\{1|{\rm Al}|1\}$, $\{1|{\rm Al}|5\}$ and $\{3|{\rm Al}|3\}$ with $L = 2\bar{\lambda}_{\rm F}$

metal/dielectric work functions are defined in the form

$$W = -\varepsilon_{\rm F}, \tag{18}$$

$$W_{\rm d}^{\rm l,r} = -\varepsilon_{\rm F}(\epsilon_{\rm l,r}, \chi^{\rm l,r}) - \chi^{\rm l,r}. \tag{19}$$

There are two situations, when $|\varepsilon_{\rm F}| > \chi^{\rm l,r}$ and $\leq \chi^{\rm l,r}$. The value $W_{\rm d}$ is the Schottky barrier height.

3. Results and Discussion

We perform calculations for both polycrystalline and crystalline films made of Na, Al, and Pb with the electron concentration $\bar{n} = 3/4\pi r_s^3$ with the corresponding electron parameter $r_s = 3.99, 2.07$, and $2.30\ a_0$. The minimal thickness of "crystalline" sandwiches should be not less than $2d$, and d is comparable to $\bar{\lambda}_{\rm F}/2$ ($\bar{\lambda}_{\rm F} = 13.06$, 6.78, and $7.53\ a_0$ for Na, Al, and Pb, respectively).

Let us firstly perform calculations: (i) with regard for formulas (11)–(15), in which it is formally assumed that $\chi = 0$ and $v_{\rm xc} \equiv v_{\rm xc}^{\rm LD}$; (ii) using (11)–(15) and $\chi \neq 0$.

(i) For a symmetric sandwich, the effect of a dielectric coating on the surfaces is reduced to the "elongation" of the electron distribution tail and the effective potential beyond the surface of a metal (polycrystalline films $\{1|{\rm Al}|1\}$ and $\{3|{\rm Al}|3\}$ on Fig. 4). The calculations were performed for $\epsilon = 1, ..., 12$. Inside the film, one can see the Friedel oscillations of the electron density with peaks near the geometrical boundaries. The period of oscillations is close to $\frac{1}{2}\bar{\lambda}_{\rm F}$ and only weakly depends on the presence of dielectric coatings. The situation is similar for Na and Pb films.

At the boundaries between the metal film and the coatings, there are jumps in the derivative of the electrostatic potential $\phi'(z)$, which disappear, provided the dielectric constants of the coatings are equal to 1. These jumps are due to the boundary conditions (A2) at $z = \pm L/2$. The jumps are also reflected on the $v_{\rm eff}(z)$ profile, since $\phi(z)$ is one of its components. In addition, at the borders, there are another jumps of not only the derivative $v'_{\rm eff}(z)$, but also of $v_{\rm eff}(z)$ profile itself for any values of ϵ, including $\epsilon = 1$. Such jumps have another origin compared to the first ones. This fact is linked to some features of the model [30], namely to the presence of the effective potential component $\langle \delta v \rangle_{\rm face}\, \theta(L/2 - |z|)$. These nonphysical jumps should not be taken into account in the estimation of the effective force

$$\mathbf{F}_{\rm eff}(z) \equiv -\nabla v_{\rm eff}(z).$$

It is seen from Fig. 4 that the force orientations are opposite at both sides of the film, so that the film on the whole must be stressed. The existence of the force should lead to an increase of the spacings between some lattice planes d, while the spacings between other planes must become narrower.

The depth of the potential well, in which the electrons are located in a metal film, decreases "on the average" with increasing ϵ and, as a result, the electron work function $W = -\varepsilon_{\rm F}(\epsilon_{\rm l,r}, \chi^{\rm l,r} = 0)$ also decreases (see Fig. 5).

The film $\{1|{\rm Al}_L|1\}$ spectra are presented in Fig. 5. For comparison, in the same figure, we also show the

results obtained within the electrons-in-a-box model with the well depth $U_0 = -(W_0 + \bar{\varepsilon}_{\rm F}) < 0$.

It is seen from Fig. 5 that the dependence of the eigenstate energies on the film thickness, within the SJ model, is oscillating and decreasing. For subbands with large numbers $i = 10, 11$, there are gaps due to the algorithm instability in a vicinity of the vacuum level. Within the rectangular-box model, this dependence is only decreasing. Due to smoother edges of the self-consistent well, it contains more subbands compared to the model of a rectangular box. Difference in subbands numbers significantly affects the calculated dielectric function and the optical conductivity of a nanofilm [14].

Within the rectangular-box model, in contrast to the SJ model, $\varepsilon_{\rm F}(L)$ is always located above one for a 3D metal. The amplitudes of oscillations decrease as L increases. Within both models, the maximum Fermi energies (minimum work functions (18)) correspond to the points, at which the curves of eigenenergies intersect Fermi energies. Within the SJ model, in contrast to the rectangular-box model, the minimum Fermi energies correspond to the points, at which the Fermi energy is located between two nearest eigenenergies (magic film thicknesses similar to magic numbers in clusters).

The asymmetric sandwiches $\{\epsilon_{\rm l}|{\rm Me}|\epsilon_{\rm r}\}$ and $\{1|{\rm Me}|\epsilon\}$, which are in contact with air or vacuum, are of particular interest from the viewpoint of experimental investigations due to the perspective of their use in technological applications (see, for example, [5]).

Let us consider both the electron density and potential profiles for the polycrystalline film $\{1|{\rm Al}|5\}$. The presence of a dielectric at the right side of the film leads to the asymmetry of the electron distribution (see the insets in Fig. 4), so that there appears a hump in both the electrostatic and effective potentials at the left side above the vacuum level. This should result, for example, in the anisotropy of a field emission along the z-axis. It is worth noting that the bottoms of wells for sandwiches $\{1|{\rm Al}|5\}$ and $\{3|{\rm Al}|3\}$ are essentially the same, some difference appears only in the "tails" of potential profiles.

It is of interest to compare the heights of humps at $L = 10, 12, 13.5$ and 20, 22, 23.5 a_0. These thicknesses correspond to the minimum and maximum of the dependence $W(L)$ for $\{1|{\rm Al}|5\}$. It turns out that, with the increase of L, the hump height weakly oscil-

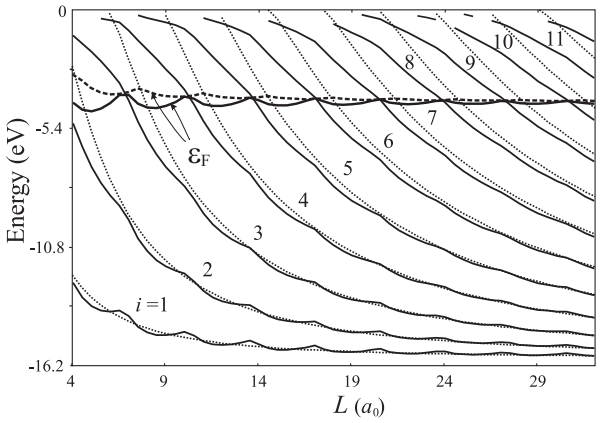

Fig. 5. Results of calculations for the energy spectrum (subbands) and the Fermi energy $\varepsilon_{\rm F}(L)$ of the film $\{1|{\rm Al}|1\}$ by the self-consistent method (solid lines) and in the rectangular-box model (dashed lines)

lates and decays similarly to the work function, but the maxima of the hump height correspond to the minima of $W(L)$. For the values of L, as given above, these heights are 0.176, 0.148, 0.170 and 0.158, 0.139, 0.156 eV, respectively.

In order to analyze such a behavior of the potential profiles, it is necessary to go beyond the isotropic model based on a defined (6) distribution of the *homogeneous* positively charged background, i.e. one has to consider not only the reaction of the electron subsystem, but also the reaction of the ion subsystem to the presence of a dielectric. The spacings between the lattice planes are determined by the balance of forces from the right and left sides for each plane. A simplest realization of this idea is to disregard variations of spacings between the lattice planes and to vary the profile of the ion jellium distribution (6). We found that such a procedure leads to a significant deformation of the well bottom, but does not result in considerable changes of both the spectrum and the hump height.

Figure 6 shows the results of our calculations of the electron work function for crystalline sandwiches using expression (18). Horizontal lines correspond to semiinfinite samples. In contrast to the surface energy, the size dependences $W(L)$ have deep and pronounced minima. It is easier to analyze them using a simple model [12]. The amplitudes of largest work function "oscillations" are smaller than 0.5 eV. By considering the dependences for different metals, it is easy to see that all the differences are due to

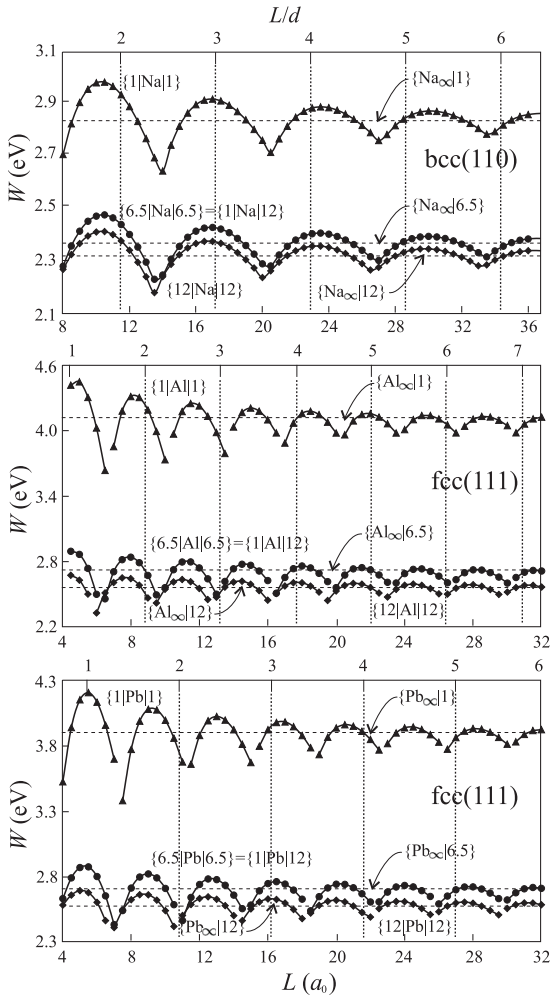

Fig. 6. Work function for crystalline sandwiches $\{\epsilon_{\rm l}|{\rm Me}|\epsilon_{\rm r}\}$ and a semiinfinite metal covered by a dielectric $\{{\rm Me}_\infty|\epsilon\}$ (Me $\equiv$ $\equiv$ Na, Al, Pb), $\chi = 0$

Table 1. **The examples of a simple coating and substrates [37, 38]**

Material	He	Ne	Ar	Kr	Xe	SiO_2	Al_2O_3	Si
ϵ	1.10	1.20	1.50	1.65	1.90	4	9	13
χ, eV	−1.0	0.10	0.20	0.45	0.68	1.1	1.35	4.05

values of r_s. For Al, which has the smallest r_s, work function oscillations are maximum, while the period is minimum. Positions of both maxima and minima depend weakly on ϵ of a dielectric and slightly shift toward smaller L with increase in ϵ.

The unexpectable result of self-consistent calculations is the coincidence of the dependences $W(L)$ for sandwiches $\{1|{\rm Me}|12\}$ and $\{6.5|{\rm Me}|6.5\}$. The computations for $\{1|{\rm Me}|5\}$ and $\{3|{\rm Me}|3\}$ give a similar result. This means that the electron work function for asymmetric sandwiches $\{\epsilon_{\rm l}|{\rm Me}|\epsilon_{\rm r}\}$ coincides with high accuracy with the work function for symmetric sandwiches $\{\langle\varepsilon\rangle|{\rm Me}|\langle\epsilon\rangle\}$ with the averaged value $\langle\epsilon\rangle = \frac{1}{2}(\epsilon_{\rm l} + \epsilon_{\rm r})$.

The work function has both the bulk and surface contributions. Because the bulk metal contributions $W(L)$ for sandwiches $\{1|{\rm Me}_L|12\}$ (like to vacuum/metal/Si) and $\{6.5|{\rm Me}_L|6.5\}$ are the same by definition. The same are the contributions of dipole surface barriers. We here imply the total contribution of both sides of a sandwich, since the work function is an "*isotropic*" characteristic [36]. The coincidence of the work functions is most likely a geometric effect. This feature will be addressed elsewhere.

The results obtained by using the developed iteration procedure enable us to draw a conclusion about its efficiency. Moreover, one can follow the behavior of electron spatial profiles and potentials, as well as calculate a spectrum. The results for $\chi = 0$ and in LDA provide reference data for simplified treatments.

(ii) Let us apply this approach ($\chi \neq 0$) to study the energetics of three samples with "ideal" interfaces: the film Al(111) on SiO_2 and on Al_2O_3, as well as the sandwich $SiO_2/Al/Al_2O_3$. For such a structure, we use the values of $\chi^{\rm l,r}$ from Table 1. $\chi^{\rm l} = 0$ and $\epsilon_{\rm l} = 1$ for the vacuum/metal interface. For illustrative purposes, we present the results of self-consistent calculations of potential profiles in Fig. 7.

It turns out that all approaches give the same potential well depth and its profile near the bottom. The dependences $v_{\rm xc}(z)$ at the left side of the film (in vacuum) are essentially the same according to approaches (i) and (ii). For the right side of the plane, they differ due to the presence of the conduction band ($\chi \neq 0$) in the dielectric.

It should be noted that the use of the nonlocal exchange-correlation potential in the iterative procedure leads to the essential disappearance of the potential hump in the effective potential (but not in the electrostatic one), which appears at the left side of the film, see Fig. 4.

In Table 2, we present our data, which correspond to scheme (ii) only. In both approaches (i) and (ii), $\varepsilon_{\rm F}$ and surface energies differ from each other by less

than 1 percent, while the values of matching parameters can be rather different: for instance, $z_0^{\rm r} = 5.95$ and $\lambda^{\rm r} = 0.998$ for ML = 1 the film Al(111) on SiO_2 of the method (i). As a result, we conclude that our manipulations with the exchange-correlation potential did not lead to any noticeable changes of the Fermi level position, i.e. $\varepsilon_{\rm F}(\langle\epsilon\rangle, \chi^{\rm l,r} = 0) \approx \varepsilon_{\rm F}(\langle\epsilon\rangle, \chi^{\rm l,r} \neq 0)$.

We also performed computations for infinite-size systems ($L = \infty$): $W_{\rm d}^{\rm r} = 2.00$ and 1.48 eV for Al/SiO_2 and Al/Al_2O_3, respectively. However, in these calculations, it is not taken into account that the vacuum/metal interface exists at the left side of the samples. Therefore, the comparison with the data of Table 2 is not possible, since the results do depend on the average dielectric constant of two media $\langle\epsilon\rangle$, and not only on $\epsilon_{\rm r}$.

Our results point out that it is possible to control the Schottky barrier by tuning the metal film thickness (in the metal-insulator-semiconductor devices, the thickness of a gate insulating film is a tool to control the current in the channel [39]). For the evaluation of the Fowler–Nordheim tunneling current [40], it is necessary to know a spatial profile of the effective potential, which should be added to the external electrostatic potential $\varphi_{\rm ext}(z)$, starting from points at $z = Z^{\rm l,r}$.

Table 2. **Calculated values for a film Al(111) of thickness L (in monolayers) on SiO_2 (upper numbers), Al_2O_3 (middle numbers), and the sandwich $SiO_2/Al/Al_2O_3$ (lower numbers)**

L [ML]	$z_0^{\rm l}$ [a_0]	$z_0^{\rm r}$ [a_0]	$\lambda^{\rm l}$ [a_0]	$\lambda^{\rm r}$ [a_0]	$W_{\rm d}^{\rm l}$ [eV]	$W_{\rm d}^{\rm r}$ [eV]	γ [J/m^2]
1	1.05	3.35	0.977	0.706	3.43	2.33	0.82
	1.00	4.25	0.962	0.518	3.01	1.66	0.76
	3.30	4.15	0.707	0.519	1.79	1.54	0.61
2	0.95	2.85	0.946	0.643	3.26	2.16	0.76
	0.95	3.60	0.945	0.474	2.84	1.49	0.70
	2.85	3.60	0.640	0.479	1.62	1.37	0.55
3	0.85	2.60	0.921	0.606	2.94	1.84	0.73
	0.85	3.50	0.919	0.476	2.63	1.28	0.70
	2.95	3.80	0.672	0.512	1.56	1.31	0.56
4	0.90	3.05	0.933	0.683	3.23	2.13	0.78
	0.95	4.05	0.948	0.531	2.86	1.51	0.74
	3.10	4.05	0.688	0.535	1.69	1.44	0.58
5	0.90	2.95	0.932	0.661	3.23	2.13	0.76
	0.95	3.85	0.948	0.507	2.84	1.49	0.72
	3.00	3.85	0.671	0.512	1.65	1.40	0.56
6	0.90	2.85	0.934	0.651	3.13	2.03	0.75
	0.90	3.65	0.933	0.489	2.73	1.38	0.71
	2.85	3.65	0.645	0.491	1.54	1.29	0.55
7	0.90	2.95	0.934	0.669	3.17	2.07	0.77
	0.90	3.90	0.933	0.520	2.80	1.45	0.73
	3.05	3.95	0.684	0.527	1.65	1.40	0.57

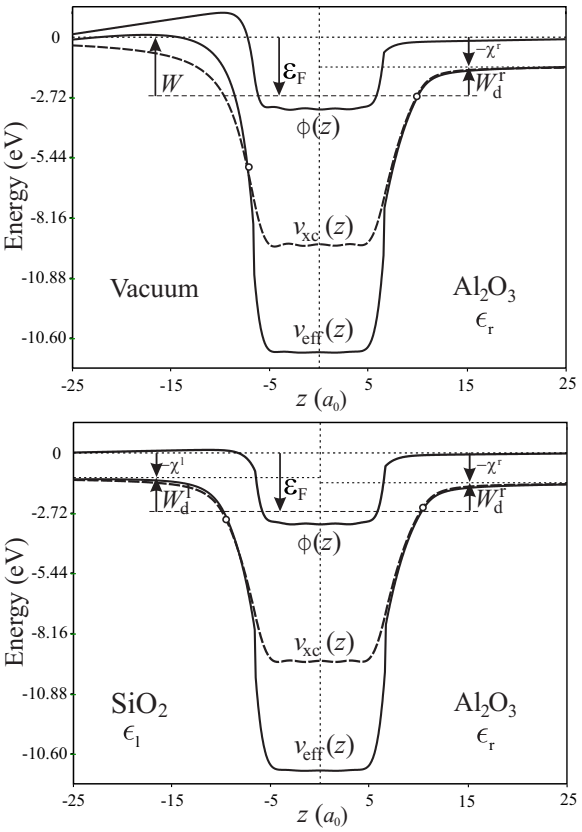

Fig. 7. Self-consistent profiles of the electrostatic, exchange-correlation and effective potentials for the sandwiches vacuum/Al(111)/Al_2O_3 and SiO_2/Al(111)/Al_2O_3. The film thickness $L = 3$ ML. 1ML = 4.4 a_0

Let us compare our results with experimental data. The calculated work function for the interface Al(111)/vacuum is 4.12 eV; the experimental one $\in (3.11, 4.26)$ eV [41]; and 4.28 eV for polycrystalline Al [42]. The recommended $\chi = 3.03$ and 3.3 eV in [43], corresponding for SiO_2 and Al_2O_3, differ from data in Table 1. The measured Schottky barrier height [43] for Au/Al_2O_3 equals 3.5 ± 0.1 eV. Note that experimental values of work function for Au and Al in Ref. [41] are close to each other, while they differ by almost 1 eV, according to Ref. [42].

On the other hand, the measured Schottky barrier heights in Ref. [44] for Al, Ag, and Cu, placed on a thick (35 nm in thickness) film of Al_2O_3, equal 1.66, 1.72, and 1.80 eV, respectively. It is in accordance with 1.5 eV for Al/Al_2O_3 [38] and the results from Table 2. As we see, experimental data are rather diverse.

An important question is about the conditions, under which our approach becomes questionable. When $|\varepsilon_F| \leq \leq \chi^{l,r}$, our model does not work. In accordance with Fig. 5 and Table 1, values $W_d \in (0.4, 0.75)$ eV for Al/Si, Pb/Si [38] and $W_d \in (0.49, 0.6)$ eV for thick films of Ti ($L \in (50, 90)$ nm) on the Si-substrate [45] should correspond to the regime $|\varepsilon_F| \leq \chi^{l,r}$. The efficient approach in this case is the local density formalism pseudopotential method [46–49]. In our approach, it is also not possible to consider the role of virtual gap states and defects in metal-dielectric contacts [50]. Nevertheless, we expect that our method provides a correct estimate for the size dependence of characteristics of films in contact with dielectrics, for which ϵ and χ are not large.

We use the simplest model, in which the dielectric constant is approximated by the step function. This approximation grasps main physical properties of the system. However, the dielectric constant should be a function of the coordinate, $\epsilon(z)$. In order to make the model more realistic, one can replace the step function by the smooth distribution $\epsilon(z)$ with variational parameters. As a result, the obtained dependences on ϵ should be weaker. From our experience, we expect that such a modification should lead to the weaker effect.

The effect of the temperature was studied earlier in Ref. [26], when determining the ionization potential of a metallic cluster. It turns out that the effect is not significant at room temperature, as it can be expected. For the film-dielectric contact, of importance is the ratio of $-\chi^r$ and the Fermi energy. If these quantities are comparable, the result should be sensitive to the temperature of the system.

4. Summary and Conclusions

We have proposed a method for self-consistent calculations of the spectra, electron work function, and surface energy of metal films placed into passive dielectrics. As typical examples, we considered Na, Al, and Pb films.

The effective force acting on the film from outside is due to the inhomogeneous electron distribution. This force should lead to the film stressing in a transverse direction. The effect of the stressing generally becomes more significant with increase in the film thickness.

In contrast to the surface energy, the size dependences of the work function have deep and strongly pronounced minima. The smaller r_s, the more difficult the problem of numerical analysis of the size dependences in vicinities of these minima.

With increase in the film thickness up to a few $\bar{\lambda}_F$, size variations of both the work function and the surface energy occur near their average values (for symmetric sandwiches, these values correspond to 3D metals and do not contain significant monotonous size contributions). A dielectric environment generally leads to a decrease of the electron work function and the surface energy.

We also considered asymmetric metal-dielectric sandwiches with different dielectrics at both sides of the film. One of the examples of such systems is a film on a dielectric substrate. We found that the presence of a dielectric from one side of the film leads to such a "deformation" of the electron distribution that there appears a "hump" above the vacuum level both in the electrostatic and effective potentials. The potential profile asymmetry should lead to an anisotropy of the field emission. In addition to the size dependences, the shift of the work function is generally determined by the average dielectric constants of environments.

We introduced the position of the conduction band in a dielectric as a parameter in the self-consistency procedure and performed calculations for the aluminum film on SiO_2 and Al_2O_3, using a nonlocal exchange-correlation potential. As a result, the profiles of electron concentration, the effective potential, and the energy spectrum are calculated.

Finally, let us formulate some methodological conclusions:

(i) The introduction of a nonlocal potential, as well as the position of the conduction band in a dielectric material does not lead to significant changes of the Fermi level of a metal film contacting with a dielectric.

(ii) Accounting for the conduction band in a dielectric and self-consistency condition for the potential well shape, one changes the spectrum (subbands number), as well as the density of states. Therefore,

the matrix elements of optical transitions are also changed, which leads to a modification of the optical absorption coefficient [14]. The equilibrium profile of electrons and the electrostatic potential are involved in the calculation of the field emission of electrons, as well as annihilation characteristics of positrons in nanostructures.

We thank V.V. Pogosov and P.V. Vakula for reading the manuscript.

APPENDIX A
Self-consistent procedure

The initial approximation $n(z)$ is chosen for solving the Kohn–Sham equations in the form of a one-parametric trial function $n^{(0)}(z) = \bar{n}\Phi(z)$, where

$$\Phi(z) = \begin{cases} -\frac{1}{2}e^{(z-L/2)/\lambda} + \frac{1}{2}e^{(z+L/2)/\lambda}, & z < -L/2, \\ 1 - \frac{1}{2}e^{(z-L/2)/\lambda} - \frac{1}{2}e^{-(z+L/2)/\lambda}, & |z| < L/2, \\ -\frac{1}{2}e^{-(z+L/2)/\lambda} + \frac{1}{2}e^{-(z-L/2)/\lambda}, & z > L/2, \end{cases}$$

λ is a variational parameter, which is found through the minimization of the surface energy. The solution by a direct variational method is an independent problem, which is not addressed in this paper (for simple metals, λ is closed to $1\,a_0$). As a result of the integration of Eq. (9) within the initial approximation, we obtain $\phi^{(0)}(z) = -4\pi\bar{n}\lambda^2\Phi(z)$.

Each wave function $\psi(z)$ is constructed as

$$\psi(z) = \begin{cases} \psi_{\text{left}}(z), & z < z_0, \\ \psi_{\text{right}}(z), & z > z_0, \end{cases}$$

under the condition of continuity of the functions $\psi_{\text{left}}(z_0) = \psi_{\text{right}}(z_0)$, as well as of their derivatives $\psi'_{\text{left}}(z_0) = \psi'_{\text{right}}(z_0)$. z_0 is an arbitrary point in the interval $z \in [-L/2; +L/2]$, while $\psi_{\text{left}}(z)$ and $\psi_{\text{right}}(z)$ are functions, which are found by the numerical solution of Eq. (7) by the Numerov's method from $z = z_-$ to $z = z_0$ and from $z = z_+$ to $z = z_0$, respectively. It is sufficient to take values $z_\mp = \mp(L + 20)\,a_0$. At these points, the potential profile $v_{\text{eff}}(z)$ is cut off. The boundary conditions (7) here are determined by the behavior of the wave function ψ under the barrier from the left ($e^{z\sqrt{|\varepsilon_i|}}$) and right ($e^{-z\sqrt{|\varepsilon_i|}}$) sides from the slab ($|z| \geq |z_\mp|$), respectively. Boundary conditions provide the wave function, as well as its derivative, at $z = z_\mp$. This peculiarity of our computations is due to the fact that the errors of the numerical method for the wave function $\psi_{\text{right}}(z)$ and $\psi_{\text{left}}(z)$ near the right and left boundaries of the interval grow, since the round-off errors also increase and lead to the instability of the algorithm under the motion toward the exponential damping.

In order to solve the system of equations (7), (9), and (16) self-consistently with a relatively small number of iteration steps, the Poisson equation (9) should be modified, in particular, by introducing a perturbation [51].

Equation (9) is solved by the Lagrange method in the form

$$\phi^{(j)\,\prime\prime} - q^2\phi^{(j-1)} = -\frac{4\pi}{f(z)}\left[n^{(j)} - \rho\right] - q^2\phi^{(j-1)} \tag{A1}$$

with the boundary conditions

$$\begin{aligned} &\phi^{(j)}_{\text{out}}\left(-\tfrac{L}{2}\right) = \phi^{(j)}_{\text{in}}\left(-\tfrac{L}{2}\right),\ \phi^{(j)}_{\text{out}}(\mp\infty) = 0, \\ &\epsilon_{\text{l}}\phi^{(j)\,\prime}_{\text{out}}\left(-\tfrac{L}{2}\right) = \phi^{(j)\,\prime}_{\text{in}}\left(-\tfrac{L}{2}\right),\ \phi^{(j)\,\prime}_{\text{out}}(\mp\infty) = 0, \\ &\phi^{(j)}_{\text{in}}\left(\tfrac{L}{2}\right) = \phi^{(j)}_{\text{out}}\left(\tfrac{L}{2}\right),\ \phi^{(j)\,\prime}_{\text{in}}\left(\tfrac{L}{2}\right) = \epsilon_{\text{r}}\phi^{(j)\,\prime}_{\text{out}}\left(\tfrac{L}{2}\right). \end{aligned} \tag{A2}$$

The term $q^2\phi$ was introduced as a small perturbation; $\phi_{\text{out}}(z)$ and $\phi_{\text{in}}(z)$ are the potentials outside and inside the film, respectively. In Eq. (A1), at each step of the iteration $j = 1, 2, 3, \ldots$, the electrostatic potential profile depends not only on the electronic concentration profile, but also on its own profile at the previous iteration. It is convenient to take q equal to the electron wave number at the Fermi sphere $\bar{k}_{\text{F}} = (3\pi^2\bar{n})^{1/3}$ of a homogeneous electron liquid.

In view of the multimolecular thicknesses of dielectric coatings on the metal film surfaces and the rapid fall of the electron distribution outside a film (approximately at a distance of 10–15 a_0), we formally neglected the effect of the thickness of the coatings, whose minimum thicknesses must be much greater than that of a monatomic (molecular) layer of a dielectric. The solution of Eq. (A1) for $\mathcal{L} \to \infty$ has the simple form

$$\phi^{(j)}(z) = \begin{cases} \left(\int\limits_{-\infty}^{z} \frac{e^{-qz'}}{2q} f_1\,dz' + A_1\right) e^{qz} + \\ + \left(-\int\limits_{-\infty}^{z} \frac{e^{qz'}}{2q} f_1\,dz' + B_1\right) e^{-qz}, & z < -L/2, \\ \left(\int\limits_{-L/2}^{z} \frac{e^{-qz'}}{2q} f_2\,dz' + A_2\right) e^{qz} + \\ + \left(-\int\limits_{-L/2}^{z} \frac{e^{qz'}}{2q} f_2\,dz' + B_2\right) e^{-qz}, & |z| \leq L/2, \\ \left(-\int\limits_{z}^{\infty} \frac{e^{-qz'}}{2q} f_3\,dz' + A_3\right) e^{qz} + \\ + \left(\int\limits_{z}^{\infty} \frac{e^{qz'}}{2q} f_3\,dz' + B_3\right) e^{-qz}, & z > L/2, \end{cases} \tag{A3}$$

where $f_m(z') = -4\pi[n(z') - \rho(z')]D_m - q^2\phi^{(j-1)}(z')$ and $D_m = \epsilon_{\text{l}}^{-1}$, 1, ϵ_{r}^{-1} for $m = 1, 2, 3$, respectively. The choice of values $B_1 = 0$ and $A_3 = 0$ immediately follows from the condition of finiteness of the potentials far away from the film.

The values of coefficients A and B are found from the solution of the system of equations (A2):

$$A_1 = \frac{2A_2}{1+\epsilon_{\text{l}}} + \frac{1-\epsilon_{\text{l}}}{1+\epsilon_{\text{l}}} \int\limits_{-\infty}^{-L/2} \frac{e^{q(z'+L)}}{2q} f_1\,dz' - \int\limits_{-\infty}^{-L/2} \frac{e^{-qz'}}{2q} f_1\,dz',$$

$$B_3 = \frac{2B_2}{1+\epsilon_{\text{r}}} - \frac{1}{1+\epsilon_{\text{r}}} \int\limits_{-L/2}^{L/2} \frac{e^{qz'}}{q} f_2\,dz' +$$

$$+\frac{1-\epsilon_{\rm r}}{1+\epsilon_{\rm r}}\int\limits_{L/2}^{\infty}\frac{e^{-q(z'-L)}}{2q}f_3dz' - \int\limits_{L/2}^{\infty}\frac{e^{qz'}}{2q}f_3dz'.$$

Let us introduce the notation

$$J_{(\pm)} = Y_0\Bigg[Y_1 2\epsilon_{\rm l}(1\mp\epsilon_{\rm r})\int\limits_{-\infty}^{-L/2}dz'e^{qz'}f_1 +$$

$$+\ Y_2(1\pm\epsilon_{\rm l})(1+\epsilon_{\rm r})\int\limits_{-L/2}^{L/2}dz'e^{-qz'}f_2 +$$

$$+\ Y_3(1\pm\epsilon_{\rm l})(1-\epsilon_{\rm r})\int\limits_{-L/2}^{L/2}dz'e^{qz'}f_2 +$$

$$+Y_4 2\epsilon_{\rm r}(1\pm\epsilon_{\rm l})\int\limits_{L/2}^{\infty}dz'e^{-qz'}f_3\Bigg],$$

where $Y_0 = \{2q[(1-\epsilon_{\rm l})(1-\epsilon_{\rm r})e^{-qL} - (1+\epsilon_{\rm l})(1+\epsilon_{\rm r})e^{qL}]\}^{-1}$. Then $A_2 = J_{(+)}$ for $Y_{1,3} = 1$, $Y_{2,4} = e^{qL}$ and $B_2 = J_{(-)}$ for $Y_{2,4} = 1$, $Y_1 = e^{qL} = Y_3^{-1}$.

In the case of the symmetric sandwich $\epsilon_{\rm l} = \epsilon_{\rm r}$, the accuracy of calculations is verified by the examination of the stationarity conditions $n'(z) = 0$ and $\phi_{\rm in}^{(i)'}(z) = 0$ at the center of the slab ($z = 0$).

1. R. Otero, A.L. Vazquez de Parga, and R. Miranda, Phys. Rev. B **66**, 115401 (2002).
2. J.J. Paggel, C.M., Wei, M.Y. Chou, D.-A. Luh, T. Miller, and T.-C. Chiang, Phys. Rev. B **66**, 233403 (2002).
3. D.V. Buturovich, M.V. Kuz'min, M.V. Loginov, and M.A. Mittsev, Phys. Solid State **48**, 2205 (2006); Phys. Solid State **50**, 173 (2008).
4. Y. Liu, J.J. Paggel, M.H. Upton, T. Miller, and T.-C. Chiang, Phys. Rev. B **78**, 235437 (2008).
5. T.-C. Chiang, AAPPS Bullet. **18**, 2 (2008).
6. A.L. Vazquez de Parga, J.J. Hinarejos, F. Calleja, J. Camarero, R. Otero, and R. Miranda, Surf. Sci. **603**, 1389 (2009).
7. N.A. Vinogradov, D.E. Marchenko, A.M. Shikin, V.K. Adamchuk, and O. Rader, Phys. Sol. State **51**, 179 (2009).
8. P.-W. Chen, Y.-H. Lu, T.-R. Chang, C.-B. Wang, L.-Y. Liang, C.-H. Lin, C.-M. Cheng, K.-D. Tsuei, H.-T. Jeng, and S.-J. Tang, Phys. Rev. B **84**, 205401 (2011).
9. E. Ogando, N. Zabala, E.V. Chulkov, and M.J. Puska, Phys. Rev. B **71**, 205401 (2005).
10. J.P. Rogers III, P.H. Cutler, T.E. Feuchtwang, and A.A. Lucas, Surf. Sci. **181**, 436 (1987).
11. M.V. Moskalets, JETP Lett. **62**, 719 (1995).
12. V.V. Pogosov, V.P. Kurbatsky, and E.V. Vasyutin, Phys. Rev. B **71**, 195410 (2005).
13. Y. Han and D.-J. Liu, Phys. Rev. B **80**, 155404 (2009).
14. V.P. Kurbatsky and V.V. Pogosov, Phys. Rev. B **81**, 155404 (2010).
15. V.D. Dymnikov, Phys. Sol. State **53**, 901 (2011).
16. F.K. Schulte, Surf. Sci. **55**, 427 (1976).
17. N. Zabala, M.J. Puska, and R.M. Nieminen, Phys. Rev. B **59**, 12652 (1999).
18. I. Sarria, C. Henriques, C. Fiolhais, and J.M. Pitarke, Phys. Rev. B **62**, 1699 (2000).
19. А.Н. Смогунов, Л.И. Куркина, О.В. Фарберович, ФТТ **42**, 1898 (2000).
20. C.M. Horowitz, L.A. Constantin, C.R. Proetto, and J.M. Pitarke, Phys. Rev. B **80**, 235101 (2009).
21. P.J. Feibelman and D.R. Hamann, Phys. Rev. B **29**, 6463 (1984).
22. J.C. Boettger, Phys. Rev. B **53**, 13133 (1996).
23. Z. Zhang, Q. Niu, and C.-K. Shih, Phys. Rev. Lett. **80**, 5381 (1998).
24. A. Kiejna, J. Peisert, and P. Scharoch, Surf. Sci. **432**, 54 (1999).
25. V.V. Pogosov, Sol. St. Commun. **75**, 469 (1990).
26. A. Kiejna and V.V. Pogosov, J. Phys.: Cond. Matter **8**, 4245 (1996).
27. K. Hirabayashi, Phys. Rev. B **3**, 4023 (1971).
28. M.J. Puska, R.M. Nieminen, and M. Manninen, Phys. Rev. B **31**, 3486 (1985).
29. A. Rubio and L. Serra, Phys. Rev. B **48**, 18222 (1993).
30. J.P. Perdew, H.Q. Tran, and E.D. Smith, Phys. Rev. B **42**, 11627 (1990).
31. J.P. Perdew and A. Zunger, Phys. Rev. B **23**, 5048 (1981).
32. A.V. Babich and V.V. Pogosov, Surf. Sci. **603**, 2393 (2009).
33. P.A. Serena, J.M. Soler, and N. Garcia, Phys. Rev. B **34**, 6767 (1986).
34. L.A. Constantin and J.M. Pitarke, Phys. Rev. B **83**, 075116 (2011).
35. A.M. Gabovich, Chem. Phys. Technol. Surf. **1**, 72 (2010).
36. V.V. Pogosov and V.P. Kurbatsky, J. Exp. Theor. Phys. **92**, 304 (2001).
37. P. Stampfli, Phys. Rep. **255**, 1 (1995).
38. E.H. Rhoderick, *Metal-Semiconductor Contacts* (Clarendon Press, Oxford, 1978).
39. L. Lin, H. Li, and J. Robertson, Appl. Phys. Lett. **101**, 172907 (2012).
40. R.H. Fowler and L. Nordheim, Proc. Roy. Soc. A **119**, 173 (1928).
41. V.S. Fomenko, *Emission Properties of Materials* (Naukova Dumka, Kiev, 1980) (in Russian).
42. H.B. Michaelson, J. Appl. Phys. **48**, 4729 (1977).
43. J.C. Brewer, R.J. Walters, L.D. Bell, D.B. Farmer, R.G. Gordon, and H.A. Atwater, Appl. Phys. Lett. **85**, 4133 (2004).
44. K. Singh and S.N.A. Hammond, Tur. J. of Phys. **22**, 315 (1998).
45. Moongyu Jang and Junghwan Lee, ETRI J. **24**, 461 (2002).
46. S.G. Louie and M.L. Cohen, Phys. Rev. B **13**, 2461 (1976).
47. G. Bordier and C. Noguera, Phys. Rev. B **44**, 6361 (1991).

48. V.G. Zavodinsky and I.A. Kuyanov, J. Appl. Phys. **81**, 2715 (1997).
49. P.W. Peacock and J. Robertson, J. Appl. Phys. **92**, 4712 (2002).
50. W. Mönch, Phys. Rev. Lett. **58**, 1260 (1987).
51. J. Arponen, P. Hautojärvi, R. Nieminen, and E. Pajanne, J. Phys. F **3**, 2092 (1973).

Received 27.03.13

А.В. Бабіч

ПРО РОБОТУ ВИХОДУ І ВИСОТУ БАР'ЄРА ШОТТКІ МЕТАЛЕВИХ НАНОПЛІВОК В ДІЕЛЕКТРИЧНОМУ КОНФАЙНМЕНТІ

Р е з ю м е

Запропоновано метод самоузгоджених обчислень характеристик металевої плівки в діелектриках. У межах модифікованого методу Кона–Шема і моделі стабільного желе розглянуто найцікавіший випадок асиметричних метал-діелектричних сандвічів, для яких діелектрики різні по обидві сторони плівки. Для полі- і монокристалічних плівок Na, Al і Pb, поміщених у пасивні ізолятори, обчислено спектр, роботу виходу електронів і поверхневу енергію. Діелектричне оточення в цілому приводить до зменшення як роботи виходу електронів, так і поверхневої енергії. Виявлено, що зміна роботи виходу визначається середньоарифметичним значенням діелектричних констант по обидві сторони плівки. У самоузгодженій процедурі як параметр було введено положення зони провідності діелектрика. З урахуванням сил зображення було виконано обчислення для наноплівок алюмінію з ідеальними інтерфейсами вакуум/Al(111) /SiO_2, вакуум/Al(111) /Al_2O_3 і сандвіча SiO_2/Al(111)/Al_2O_3. В результаті було розраховано профілі ефективних потенціалів і висоти бар'єрів Шоттки.

А.В. Бабич

О РАБОТЕ ВЫХОДА И ВЫСОТЕ БАРЬЕРА ШОТТКИ МЕТАЛЛИЧЕСКИХ НАНОПЛЕНОК В ДИЭЛЕКТРИЧЕСКОМ КОНФАЙНМЕНТЕ

Р е з ю м е

Предложен метод самосогласованных вычислений характеристик металлической пленки в диэлектриках. В рамках модифицированного метода Кона–Шэма и модели стабильного желе рассмотрен наиболее интересный случай асимметричных металл-диэлектрических сандвичей, для которых диэлектрики разные по обе стороны пленки. Для полии монокристаллических пленок Na, Al и Pb, помещенных в пассивные изоляторы, вычислены спектр, работа выхода электронов и поверхностная энергия. Диэлектрическое окружение в целом приводит к уменьшению как работы выхода электронов, так и поверхностной энергии. Выявлено, что изменение работы выхода определяется среднеарифметическим значением диэлектрических констант по обе стороны пленки. В самосогласованной процедуре как параметр было введено положение зоны проводимости диэлектрика. С учетом сил изображения были выполнены вычисления для нанопленок алюминия с идеальными интерфейсами вакуум/Al(111)/SiO_2, вакуум/Al(111)/Al_2O_3 и сандвича SiO_2/Al(111)/Al_2O_3. В результате были рассчитаны профили эффективных потенциалов и высоты барьеров Шоттки.